STATISTICAL TOOL SIZE STUDY FOR COMPUTER CONTROLLED OPTICAL SURFACING

by

Weslin Charles Pullen

A Thesis Submitted to the Faculty of the

JAMES C WYANT COLLEGE OF OPTICAL SCIENCES AND ENGINEERING

In Partial Fulfillment of the Requirements
For the Degree of

MASTER OF SCIENCE

In the Graduate College

THE UNIVERSITY OF ARIZONA

2022

THE UNIVERSITY OF ARIZONA
GRADUATE COLLEGE

As members of the Dissertation Committee, we certify that we have read the thesis prepared by Weslin Charles Pullen, titled Statistical tool size study for computer controlled optical surfacing and recommend that it be accepted as fulfilling the thesis requirement for the Degree of Master of Science.

Date: April 26, 2022
Daewook Kim

Hubert Martin
Date: April 26, 2022
Hubert (Buddy) Martin

Date: April 26, 2022
Chang Jin Oh

Date: April 26, 2022

Date: April 26, 2022

Date: April 26, 2022

Final approval and acceptance of this thesis is contingent upon the candidate's submission of the final copies of the thesis to the Graduate College.

I hereby certify that I have read this thesis prepared under my direction and recommend that it be accepted as fulfilling the thesis requirement.

Date: April 26, 2022
Dissertation Director: Daewook Kim

STATEMENT BY AUTHOR

SIGNED: Weslin Pullen

Weslin Charles Pullen

APPROVAL BY THESIS DIRECTOR

This thesis has been approved on the date shown below:

May 12, 2022

Daewook Kim
Associate Professor of Optical Sciences

Date

ACKNOWLEDGEMENTS

First and foremost, thanks to Jim Burge, who unknowingly inspired this topic while I sat in his office watching him determine tool sizes to use based on surface profiles I gave him. Thanks to Daewook for encouraging me to keep looking for something fun and novel to explore, and for allowing me time to balance family, work and school. Thanks to my boys (Caleb, Triston, Owen and Miles) for letting me study when they really just wanted to play with Dad. And, most importantly, thanks to my amazing wife, Nicole, for putting up with the added stress I caused by pursuing a Masters while working full-time with four kids at home, to let me chase my dreams.

DEDICATION

To my kids. May you always question the way things work, come up with cool ideas to make things better, try and fail, learn from failure and try again.

TABLE OF CONTENTS

LIST OF FIGURES

ABSTRACT

Over the past few decades, Computer Controlled Optical Surfacing (CCOS) systems have become more deterministic. A target surface profile can be predictably achieved by a combination of tools of different sizes. However, deciding the optimal set of tool sizes that will achieve the target residual error in the shortest run time is difficult and no general guidance has been proposed in the literature. In this paper, we present a computer-assisted study on choosing the proper tool sizes. First, we propose that the Characteristic Frequency Ratio (CFR) can be used as a general measure of the correction capability of a tool over a surface profile. Second, the performance of different CFRs are quantitatively studied with a computer simulation by applying them to guide the tool size selection for polishing a large number of randomly generated surface profiles with similar initial spatial frequencies and root mean square errors. Finally, we found that CFR = 0.75 achieves the most stable trade-off between the total run time and the number of iterations, and thus can be used as a general criterion in tool size selection for CCOS processes. To our best knowledge, CFR is the first criterion that ties the tool size selection to the overall efficiency.

CHAPTER 1

Introduction

Computer Controlled Optical Surfacing (CCOS) (Jones, 1977; Cheng, 2016) systems have been successfully used to fabricate high-precision optics in various cutting-edge applications, such as telescopes for space exploration (Fanson et al., 2020; Ghigo et al., 2014; Kim et al., 2021), X-ray mirrors for synchrotron radiation and free-electron laser facilities (Schindler et al., 2003; Beaucamp and Namba, 2013; Thiess et al., 2010; Wang et al., 2021a,b), and optics in EUV lithography (Weiser, 2009; Wischmeier et al., 2020). Different CCOS systems use different tools, which can be adopted based on the requirement of the precision and shape of the desired optical surface.

CCOS uses tools that are much smaller (*i.e.,* sub-aperture tools) than the optical surface to correct the local errors. All CCOS techniques are mathematically modeled and have become much more deterministic (Han et al., 2020; Chaves-Jacob et al., 2021), which enable a desired optical surface profile to be predictably achieved by a combination of tools with different sizes. In the CCOS process a tool is simulated by its material removal footprint known as its Tool Influence Function (TIF). It is well known that certain TIF sizes have a limit to the feature sizes within the optical surface that they can correct (Cheng, 2016; Zhou et al., 2009; Wang et al., 2014, 2017). Basically, larger TIFs with higher Peak Removal Rate (PRR) are preferred because they remove material faster. However, while any given TIF can correct features larger than the size of the TIF completely, they cannot correct features that are smaller than the TIF footprint well. On the other hand, if the TIF is too small, the surfacing efficiency will be low, and unexpected mid-to-high-frequency errors may be left on the optical surface. Therefore, choosing the optimal set of TIF sizes that achieves the target residual surface error with the shortest amount of run time has been a difficult problem in practical CCOS processes. This problem is especially important in the fabrication of large optics, where an small improvement of efficiency leads to a great reduction in manpower and financial resources.

Conventionally, a set of tools was empirically determined by a fabrication artisan's experience. However, multiple iterations of the trial and error cycle are usually required to approach the target residual surface error, which is inefficient. Also, this method highly relies on the expertise of the artisan and thus cannot be formalized as a general guidance.

Quantitative characterization of the correction capability of a certain TIF has been attempted by examining the Power Spectral Density (PSD) of the TIF (Zhou et al., 2009; Wang et al., 2014, 2017) in the literature. The PSD uses the Fourier transform to decompose a TIF and a surface error map into different spatial frequencies with their respective amplitudes. The amplitudes quantify the contributions of certain spatial frequencies to the entire surface error map. With the help of the PSD, Zhou *et. al.,* theoretically analyzed the removal characteristics in a CCOS process using a sinusoidal surface error map that only contains a single spatial frequency. A Material Removal Availability (MRA) equal to the ratio between the target material removal volume and the actual (or predicted) material volume removed was proposed as an indicator of the correction capability of a particular TIF (Zhou et al., 2009). MRA can be used to determine how well a TIF can correct certain spatial frequencies. However, the concept was only verified on single frequencies, and the relationship between MRA and the total run time was unclear. Wang *et. al.,* presented a procedure of using the PSD to calibrate a specific TIF to determine its capability of correcting features that are smaller than the TIF (Wang et al., 2014, 2017). However, this procedure requires multiple real fabrication runs and metrology to feed back to the result, and specifically focused on the smoothing efficiency of a TIF. Therefore, the method is not generally applicable to other TIFs without running the same procedure.

In this study, we present a computer-assisted analysis on a general guidance to choose proper tool sizes for a given surface error map. First, the concept of a Characteristic Frequency Ratio (CFR) is developed from Fourier theory and calibrated with a reference, single-frequency sinusoidal surface as a proper measure of the correction capability of a certain TIF. Second, the relationship between the CFR and the run time is quantitatively studied via massive computer simulations, where different combinations of CFRs are applied as a reference in choosing the tool sizes for a large number of randomly generated surface error maps with similar initial spatial frequencies and Root Mean Square (RMS) values. The statistics, including the average of the run time, the standard deviation of the run time, and the number of iterations, for each CFR combination are summarized and compared. Finally, the simulation results demonstrate that the CFR = 0.75 achieves the most stable trade-off between the total run time and the number of iterations, and thus can be selected as a general efficiency criterion in choosing the tool sizes in CCOS. To our best knowledge, this is the first statistical study of tool size selection, and the CFR is the first general criterion that ties the TIF correction capability to the total run time.

The rest of the paper is organized as follows. The necessary background of Fourier theory as applied to analyze surface error is briefly reviewed in Chapter 2, followed by a detailed explanation of the novel Characteristic Frequency (CF) of a TIF and its calibration in Chapter 3. Chapter 4 provides examples of determining the CF for three standard TIF shapes, then Chapter 5 describes the proposed CFR criterion. The computer-assisted study of different CFRs is discussed in Chapter 6, which includes a discussion on the practical applicability and limitation of the study. Chapter 7 concludes the paper.

CHAPTER 2

Fourier analysis on surface error

2.1 The Fourier Transform

In optical fabrication, surface errors are usually described as a 2D matrix of the difference between the measured and the target surface shapes. This surface error map consists of error features which vary in lateral size and magnitude. The Discrete Fourier Transform (DFT) of the surface error is defined as

$$\mathcal{Z}\left(u,v\right) = l_x l_y \sum_{x=0}^{N_x-1} \sum_{y=0}^{N_y-1} Z\left(x,y\right) e^{-i2\pi\left(\frac{u}{N_x}x+\frac{v}{N_y}y\right)}, \tag{2.1}$$

where $\mathcal{Z}\left(u,v\right)$ is the 2D spatial frequency spectrum of the surface error $Z\left(x,y\right)$ and $l_x \times l_y$ is the pixel size. Here $l_x = N_x/L_x$ and $l_y = N_y/L_y$ where N_x and N_y are the numbers of sample points in x- and y-direction, respectively, and L_x and L_y are the periodicity in x- and y-direction, respectively. The DFT decomposes the surface error into all the spatial frequencies which are present in the measurement, represented as sinusoidal features and their respective amplitudes.

2.2 Power Spectral Density

The Power Spectral Density (PSD) of a surface is a statistical tool that decomposes a surface into contributions from different spatial frequencies. Figure 2.1 illustrates the relationship between the measured surface profile and its one-dimensional PSD curve, namely that the PSD is the Fourier transform of the auto-correlation function of the surface error map, which contains the power across a range of frequencies. An important realization is that the PSD of the mean-removed surface error gives the surface variance of each spatial frequency present in the measurement. It is

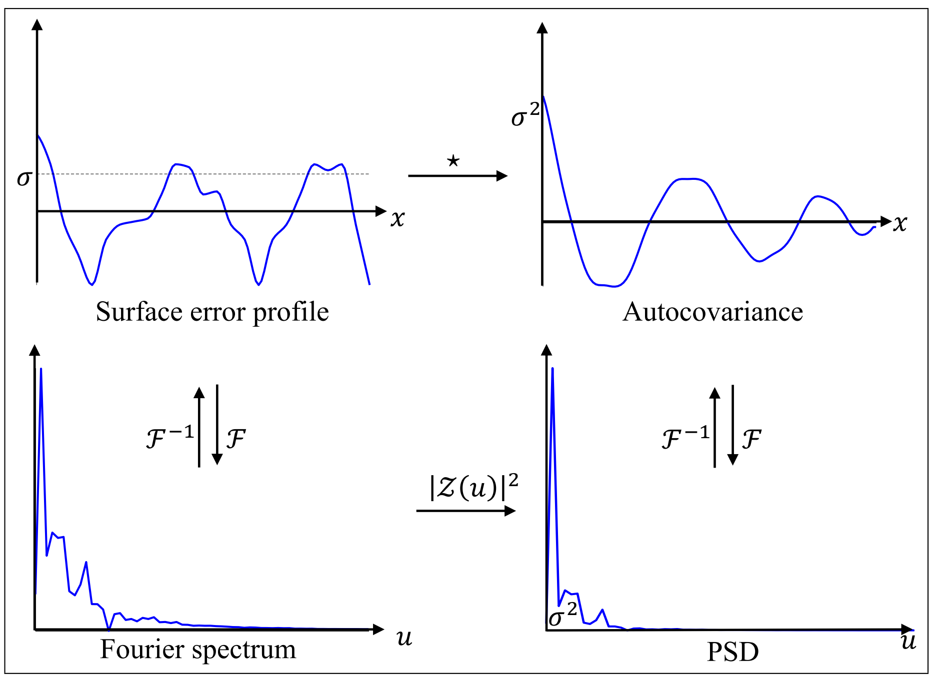

Figure 2.1: Schematic of the relationship between relevant surface parameters, where "$\star$" is the auto-correlation operator, $\mathcal{F}$ and $\mathcal{F}^{-1}$ represents the forward and inverse Fourier transforms, respectively, and σ^2 is the variance of the surface profile.

worth mentioning that in the real implementation of DFT defined in Eq. 2.1, it is assumed that $l_x = l_y = 1$ so that $1/L_xL_y = 1/N_xN_y$ (Jacobs et al., 2017). Therefore, according to Fig. 2.1, the PSD based on Eq. 2.1 can be calculated as

$$\mathcal{P}(u,v) = \frac{1}{N_xN_y}\left|\mathcal{Z}(u,v)\right|^2. \tag{2.2}$$

2.3 Encircled Error

In optical metrology the encircled energy has been used to measure the concentration of energy of a Point Spread Function (PSF) at the image plane. Analogous to the encircled energy of a PSF we define the Encircled Error (EE) of a PSD as,

$$E(r) = \frac{\sum\limits_{\theta=0}^{2\pi}\sum\limits_{\rho=0}^{r}\mathcal{P}(\rho,\theta)}{\sum\limits_{\theta=0}^{2\pi}\sum\limits_{\rho=0}^{\mathrm{R}}\mathcal{P}(\rho,\theta)}, \tag{2.3}$$

where $\mathcal{P}(\rho,\theta)$ is $\mathcal{P}(u,v)$ transformed to the polar coordinate system, ρ is the sampled frequency measured radially from the central frequency bin, θ is the azimuthal angle covering the PSD, and R is the maximum spatial frequency within the PSD. As an example, Fig. 2.2(a) shows a randomly generated surface with a total RMS error of 98.8 nm. Figure 2.2(b) is its two-dimensional (2D) PSD map and Fig. 2.2(c) gives the corresponding EE. Recalling that the PSD of the mean-removed surface error is the surface variance contribution of each spatial frequency contained in the measurement, the EE then tells what percentage of the error is due to spatial frequencies lower than a given frequency.

2.4 Characteristic Frequency of a Surface Error Map

For an optical image, a typical criterion for the encircled energy is the radius of the PSF at which 50% or 80% of the energy is encircled. As an analogy, for this study, we define the Characteristic Frequency (CF) of a given surface error map to

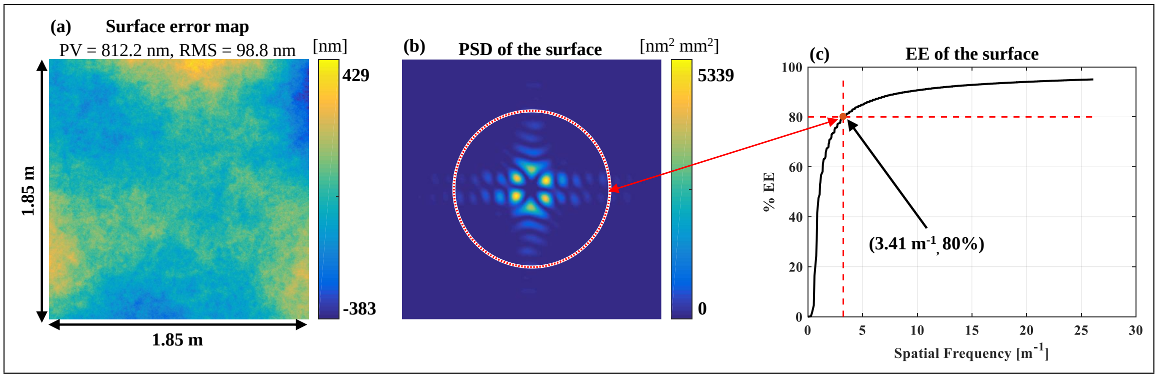

Figure 2.2: An example surface error map (a) and its 2D PSD map (b). The EE of the PSD (c) demonstrates that 80% of the RMS error is due to spatial frequencies lower than 3.24 m^{-1}.

be located at EE = 80% as

$$f^c_{SURF} = \arg_r \left[E\left(r\right) = 80\% \right], \tag{2.4}$$

where f^c_{SURF} refers to the CF of the surface error map. For example, as shown in Figs. 2.2(b) and 2.2(c), the CF of this surface error map is $f^c_{SURF} = 3.24\ \mathrm{m}^{-1}$.

CHAPTER 3

The Reference TIF

Zhou, *et. al* discussed how the amplitude frequency spectrum, given by the Fourier transform of a Tool Influence Function (TIF) is a measure of the correctability of that TIF for localized errors of the same spatial frequencies (Zhou et al., 2009). We use a reference surface and a reference TIF to calibrate the CF of the TIF.

3.1 The Reference Surface

Since the Fourier series decomposes surface errors into sinusoidal patterns, we define a reference surface error map containing a single Fourier mode in x direction as

$$Z_{REF}\left(x,y\right)=\mathrm{A}\cdot\cos\left(2\pi fx\right)+\mathrm{A}, \tag{3.1}$$

where A is the amplitude and f is the single spatial frequency of the surface error. The reference surface error map and its profile along the x-direction are shown in Figs. 3.1(a) and 3.1(b), respectively, where the size of the map is 100 mm $\times$ 100 mm, and A $=$ 10 nm and $f = 0.05\ \mathrm{mm}^{-1}$ are used in this study. It is worth mentioning that A and f can be set arbitrarily and will not affect the outcome of the analysis. Also note that the surface error is piston-adjusted to have no negative values since CCOS processes are only capable of removing material.

3.2 Preston's Equation and the Line TIF

The material removal process is classically defined by the Preston's equation (Cheng, 2016) as

$$\frac{\partial Z\left(x,y\right)}{\partial t}=\kappa\cdot P\left(x,y\right)\cdot V\left(x,y\right) \tag{3.2}$$

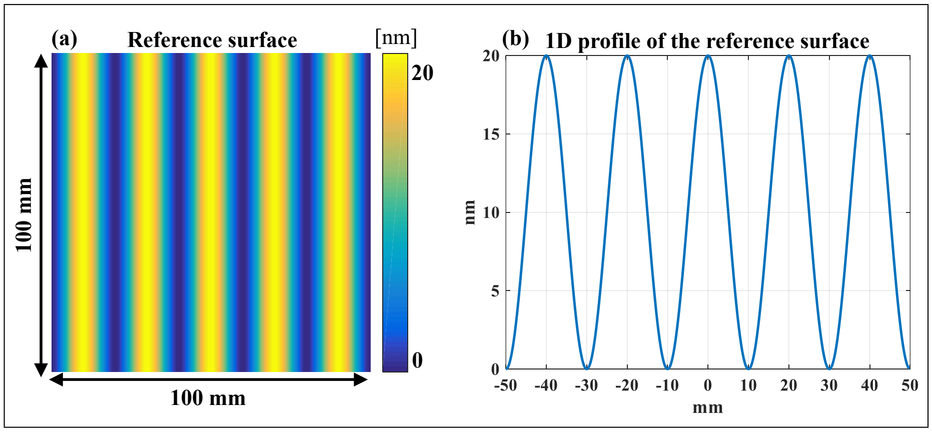

Figure 3.1: (a) The reference surface error map and (b) its 1D profile along the x-direction.

where the material removal rate per unit time, $\partial Z\left(x,y\right)/\partial t$, is proportional to the contact pressure, $P\left(x,y\right)$, and the relative velocity, $V\left(x,y\right)$, between the tool and the workpiece. The Preston's Constant, κ, is used to consider additional polishing parameters such as slurry, polishing interface, *etc.* This equation is used to theoretically define a static TIF, which gives the material removal rate of a polishing process if the tool was parked in one spot and allowed to run for one unit of time. According to Eq. 3.2, a TIF which matches the shape of the error feature will perfectly correct that error in the shortest amount of time (*i.e.,* the most efficient TIF for that feature).

The static TIF considers only the motion of the tool without traveling across the workpiece. Many CCOS processes use a spiral tool path and therefore the Ring TIF was conceived (Kim et al., 2009a). The Ring TIF considers the motion of tool travel across the workpiece as the workpiece rotates under the tool and is therefore a function of radial position from the center of the workpiece. To simplify this technique we define the Line TIF, which is defined in the same way as the Ring TIF, only a Cartesian raster tool path is assumed rather than a spiral. Converting the 2D static TIF to the Line TIF is as simple as summing down the columns (or equivalently the rows depending on the major direction of the raster path) of the static TIF matrix.

3.3 The Reference TIF

Therefore, the ideal (*i.e.*, reference) Line TIF, $I_{REF}(x, y)$, for the single-frequency surface error map is simply one period of the sinusoid of the same frequency defined as

$$I_{REF}(x, y) = \frac{\text{PRR}}{2} \cdot \cos(2\pi f x) + \frac{\text{PRR}}{2}, \ f = 0.05\text{mm}^{-1}, \tag{3.3}$$

where PRR is the peak removal rate of the TIF, and the TIF is piston-adjusted by PRR/2 so that there are no negative removal rates. It is obvious from Eqs. 3.1 and 3.3 that the ideal TIF to correct the reference surface in Fig. 3.1 is the sinusoidal reference TIF with frequency $f = 0.05$ mm^{-1}. Therefore, the CF of the reference TIF is defined as $f^c_{TIF} = 0.05$ mm^{-1}. Figure. 3.2(a) shows the 1D profile of the reference TIF in x direction with PRR = 1 nm/s.

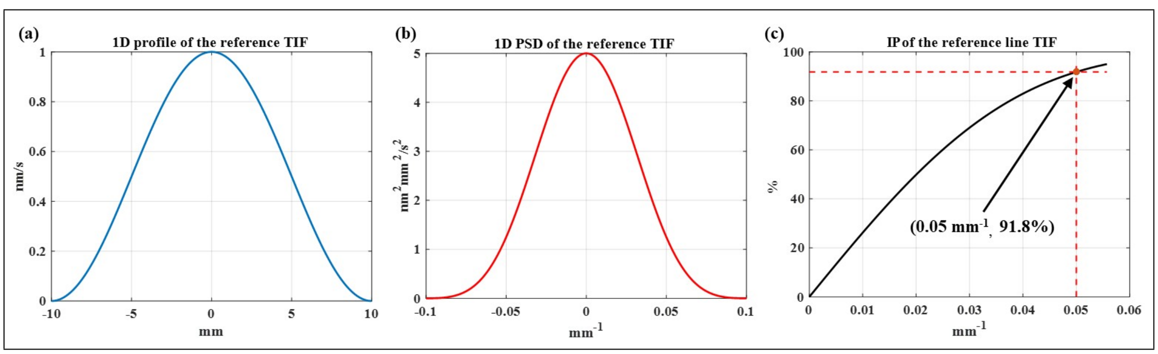

Figure 3.2: (a) Reference Line TIF with characteristic frequency $f^c_{TIF} = 0.05mm^{-1}$, (b) 1D PSD of the reference Line TIF, (c) IP of the reference TIF.

3.4 Integrated PSD and the Characteristic Frequency of a TIF

To generalize the CF to any TIF, we take the analysis from Zhou *et. al* further by defining the Integrated PSD (IP) of a TIF to calibrate a TIFs CF. As shown in Figs. 3.2(b) and 3.2(c), the IP is simply a one-dimensional (1D) equivalent of an EE calculation (see Eq. 2.3) performed on the 1D PSD of the Line TIF. For the reference TIF with $f^c_{TIF} = 0.05$ mm^{-1}, as demonstrated in Fig. 3.2(c), the corresponding IP occurs at 91.8%. Therefore, we define the CF for any TIF as the spatial frequency where IP = 91.8%, *i.e.*,

$$f^c_{TIF} = \arg_r \left[I\left(r\right) = 91.8\% \right]. \tag{3.4}$$

CHAPTER 4

Extending the calibration to other TIF shapes

Utilizing the calibration of the f^c_{TIF} (see Eq. 3.4) by means of the reference TIF illustrated in Chapter 3.1 we can determine the size of any kind of TIF by simply applying a scale factor depending on the given TIF shape. In the following subsections we provide examples that employ Eq. 3.4 to determine the appropriate size of three kinds of typical TIFs in CCOS to correct the reference surface in 3.1, namely Gaussian TIFs (Wang et al., 2021b), spin TIFs (Kim et al., 2009b), and orbital TIFs (Kim et al., 2009b), with the objective that the CF of these TIFs match the only error frequency present in the reference surface in Chapter 3.1.

4.1 The Gaussian TIF

The zero-mean, rotationally symmetric Gaussian TIF can be defined as

$$I_G(x, y) = \mathrm{PRR} \cdot \exp\left(\frac{x^2 + y^2}{2\sigma^2}\right), \tag{4.1}$$

where σ is the standard deviation of the Gaussian distribution that defines the size of the Gaussian TIF. The size of a Gaussian TIF can be defined by the Full Width at Half Maximum (FWHM), defined as $\mathrm{FWHM} = 2\sigma\sqrt{2\ln 2}$. Then the scale factor for the Gaussian TIF is FWHM/f^c_{TIF}.

4.2 The Spin TIF

The Spin TIF is derived from Eq. 3.2 as

$$I_S\left(x, y\right) = \begin{cases} \kappa \cdot P\left(x, y\right) \cdot \omega \cdot \rho\left(x, y\right), & \rho \leq \mathrm{R}_T, \\ 0, & \rho > \mathrm{R}_T \end{cases} \tag{4.2}$$

where ω is the angular velocity of the spinning motion of the machine tool, R_T is the radius of the actual tool, and $\rho(x, y)$ is the radial distance from the center of the tool. The size of the spin TIF is defined only by the size of the tool, so $\mathrm{R}_{TIF} = \mathrm{R}_T$. The scale factor for the Spin TIF is then $\mathrm{R}_{TIF}/f^c_{TIF}$.

4.3 The Orbital TIF

The orbital TIF is also derived from Eq. 3.2, but is much more complicated than the previous two TIFs. Dong, *et. al.,*, provide a well-organized derivation of the orbital TIF (Dong et al., 2014) summarized as

$$I_O(x,y) = \begin{cases} \dfrac{\pi}{30} \cdot \kappa \cdot P(x,y), & \rho \leq \mathrm{R}_T - \mathrm{R}_O, \\ \dfrac{1}{30} \cdot \kappa \cdot P(x,y) \cdot \omega \cdot \mathrm{R}_O \cdot \arccos\left(\dfrac{\rho^2(x,y) + \mathrm{R}_O^2 - \mathrm{R}_T^2}{2 \cdot \rho(x,y) \cdot \mathrm{R}_O}\right), & \mathrm{R}_T - \mathrm{R}_O < \rho \leq \mathrm{R}_T + \mathrm{R}_O \cdot \\ 0, & \rho > \mathrm{R}_T + \mathrm{R}_O \end{cases} \tag{4.3}$$

where R_O is the radius of the orbital stroke, and all the other variables are the same as presented in 4.2. Unlike the previous two TIFs, the Orbital TIF is defined by two parameters, both R_T and R_O, namely $\mathrm{R}_{TIF} = \mathrm{R}_O + \mathrm{R}_T$. Similar to the Spin TIF, the scale factor for the Orbital TIF is $\mathrm{R}_{TIF}/f^c_{TIF}$.

4.4 Determining the TIF size to match a desired CF

In order to determine the desired TIF size for a given CF, simply generate an arbitrary size TIF, calculate the scale factor and multiply by the desired CF. This procedure is demonstrated as follows. First, the 2D TIF is generated based on its governing equation described above at an arbitrary size. Next, the 1D Line TIF is obtained by summing down the columns of the 2D TIF, from which the 1D PSD is calculated. The EC is then calculated, where we can determine the f^C_{TIF} for the respective size and shape of TIF in use. Finally, the scale factor is calculated and the 2D TIF is scaled accordingly. Figure 4.1 shows the Gaussian, Spin, and Orbital TIFs scaled to have a $f^c_{TIF} = 0.05$ mm^{-1}.

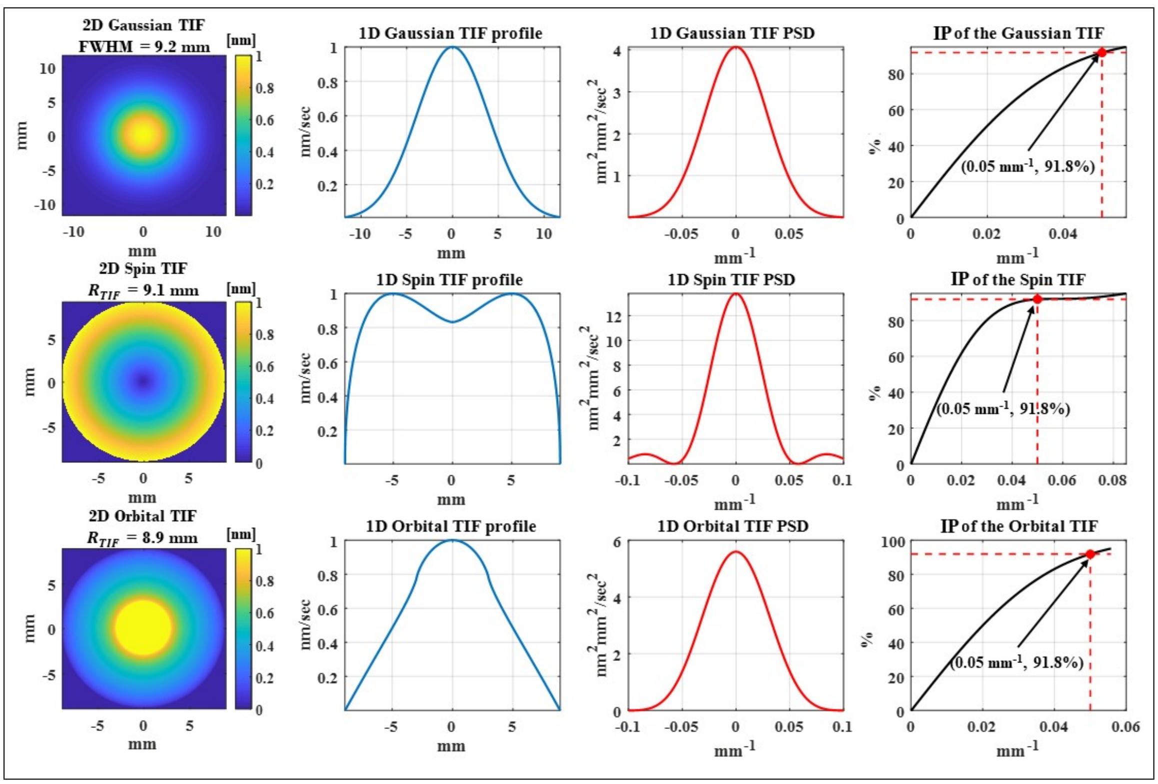

Figure 4.1: Typical TIFs scaled to have a characteristic frequency of $f_c = 0.05mm^{-1}$

CHAPTER 5

The Characteristic Frequency Ratio, a criterion for tool size selection

We have defined f_{SURF}^c for a surface error map and calibrated f_{TIF}^c for a TIF, and illustrated the method of determining the size of a TIF using f_{TIF}^c. Now we need a new criterion that can combine f_{SURF}^c with f_{TIF}^c to guide tool size selection based on a particular surface error map. To do so, we define the Characteristic Frequency Ratio (CFR), which is simply the ratio between the CF of a TIF and the CF of a surface error map, *i.e.*,

$$\text{CFR} = \frac{f_{TIF}^c}{f_{SURF}^c}. \tag{5.1}$$

This simple ratio allows us to quantitatively set the TIF size based on the spatial frequency distribution of the surface error. A CFR = 1, based on the definitions given in the previous chapters, theoretically implies that the given TIF will correct 80% of the surface error. However, this setting may cost too much processing time, negatively influencing the process efficiency. In addition, because this TIF only corrects the lower 80% frequency modes, the remaining 20% of the error is now due to higher spatial frequencies not suited for the initial TIF, so a new, smaller TIF is now required. Although the frequency content of the new residual error map has changed, the CFR should be able to be used once again to set this TIF size appropriately. Therefore, a well selected CFR for each TIF is critical for the overall accuracy and efficiency.

CHAPTER 6

Computer-assisted study of the optimal CFR for tool size selection

An optimal CFR should consider the following aspects. Firstly, it should balance the accuracy and efficiency. In other words, we expect that the target residual RMS error can be achieved in the shortest available total run time of all the tools. Secondly, the number of iterations, *i.e.,* the number of tools employed to achieve the target should be as small as possible, since the frequent change of tools also influence the overall efficiency. Finally, the selected CFR should be stable so that the same CFR can be applied to select tool size in each iteration. Based on these philosophies, a computer simulation is designed and conducted to statistically study the optimal CFR.

6.1 Simulation specification

To study the optimal CFR, different CFR values are applied to select tool sizes for many initial surface error maps that are randomly generated with the same RMS value.

In detail, similar to the surface error map shown in Fig. 3.1(a), for a single test case, we first generate a random surface error map with the size of 1.85 m $\times$ 1.85 m by using the measured PSD trend of the DKIST primary mirror (Kim et al., 2016), adding random amounts of low-to-mid-spatial frequency errors and scaling to the same total RMS.

Next, a CFR value is selected to investigate, with CFR $\in \{0.5, 0.6, 0.7, 0.8, 0.9\}$. The CFR along with the CF of the given surface error map is used to define the TIF size as detailed in Chapter 4. The Robust Iterative Fourier Transform-based dwell time Algorithm (RIFTA) (Wang et al., 2020) is used to determine the residual error and the total run time for each iteration, since RIFTA is fast and minimizes the residual and run time simultaneously. Afterwards, on the residual error map, another TIF is chosen by the same method. This procedure is repeated for this test case until the surface is within the target RMS bounds which is set to be 15% $\pm$ 3% of the initial RMS. Each test case is run 30 times and the average total run time, run time standard deviations (or $1-\sigma$), and average numbers of iterations are recorded.

The above process is repeated on a workstation computer for each CFR. Fig. 6.1 depicts one iteration of this process for CFR = 0.7.

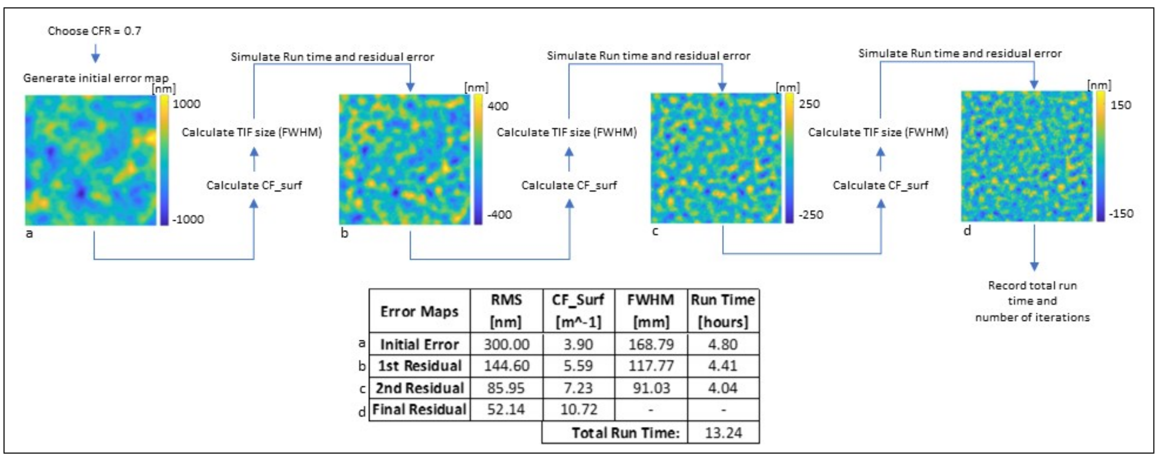

	Error Maps	RMS [nm]	CF_Surf [m^-1]	FWHM [mm]	Run Time [hours]
a	Initial Error	300.00	3.90	168.79	4.80
b	1st Residual	144.60	5.59	117.77	4.41
c	2nd Residual	85.95	7.23	91.03	4.04
d	Final Residual	52.14	10.72	-	-
			Total Run Time:		13.24

Figure 6.1: Simulation example for one iteration of test case with CFR = 0.7 showing (a) initial error map, (b) first residual error map, (c) second residual error map, and (d) final residual error map with a table keeping track of the RMS value and CF of each map, the FWHM of the Gaussian TIF used on each map, and the calculated run time required for each run.

6.2 Simulation result

The results of the simulation are shown in Fig. 6.2. To compare the results of each case, we define a Figure of Merit (FoM) for one case to be the RSS of the average run time, standard deviation of run time, and average number of iteration, each normalized by the maximum case value for its respective category. A smaller FoM value thus corresponds to a more efficient CFR. As shown in Fig. 6.2, the small FoM values appear between CFR = 0.7 and CFR = 0.8.

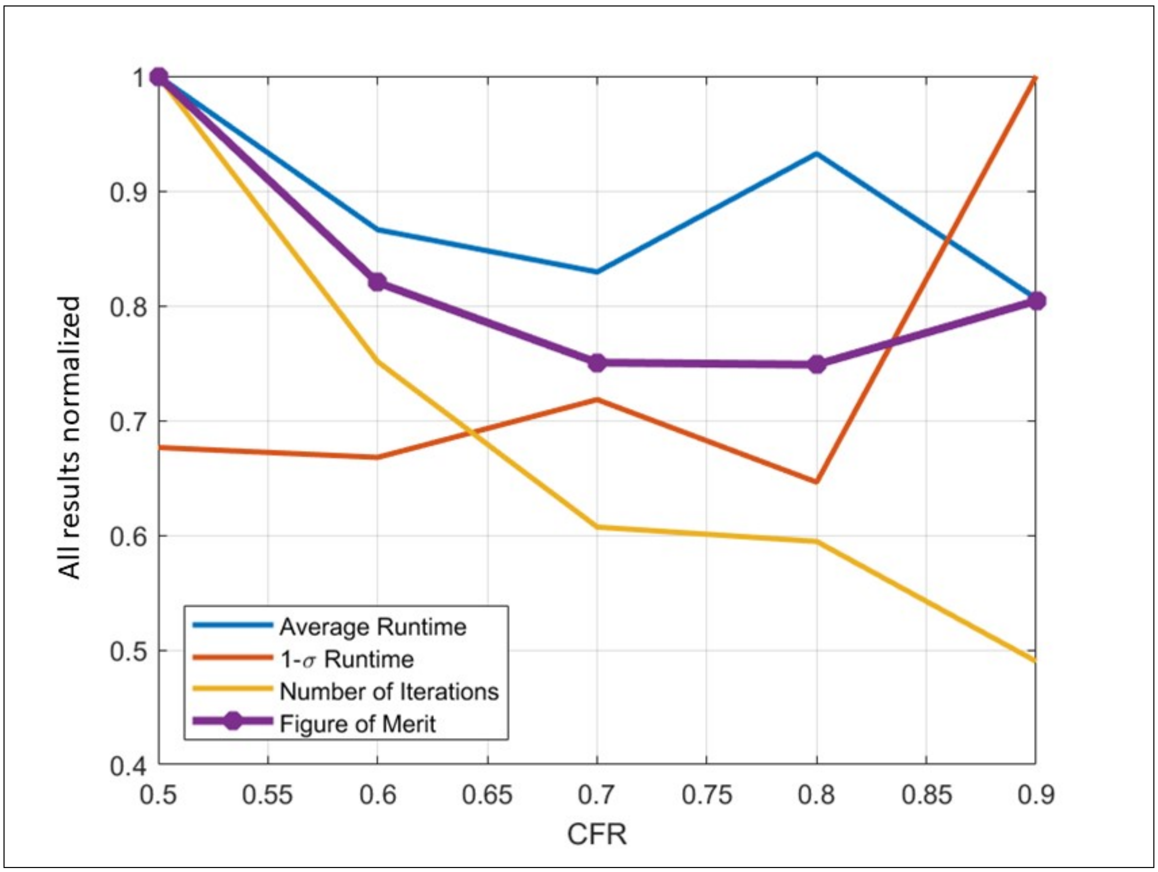

Figure 6.2: Simulation results of the average total run time (blue), the standard deviation of the total run time (red), the average number of iterations (yellow), and the Figure of Merit (purple).

The average run time of each case is studied in the blue line in Fig. 6.2, which is calculated as the mean run time of the 30 runs of the same case. It is obvious that CFR = 0.5 and CFR = 0.8 do not appear to be a good choice because of longer run time. The standard deviation of the total run time of each case is shown in red in Fig. 6.2, which represents the stability of the selected CFR. It is found that CFR = 0.9 is not very stable. Finally, the average number of iterations of each case that have been spent to achieve the target residual error is given in yellow in Fig. 6.2. A small number of iterations indicates a higher overall efficiency of the selected CFR value, primarily due to the down time caused by tool changes. Therefore, larger CFR values tend to be more efficient by this definition than smaller CFR values. It is clear by interpolation that the consistent use of a CFR between 0.75 yields the most stable balance among the accuracy, total run time and the number of required iterations, and is thus selected as a general criterion in choosing tool sizes in CCOS.

CHAPTER 7

Conclusion

In this thesis, we propose a straightforward Characteristic Frequency Ratio (CFR) to guide tool size selection in Computer Controlled Optical Surfacing (CCOS) processes. The proposed CFR is statistically studied via computer simulation, and it is the first general criterion that considers both the residual errors and total run time.

CFR is defined as the ratio between the Characteristic Frequencies (CFs) of a surface error map and a Tool Influence Function (TIF). While the CF of a surface error map is defined according to the proposed encircled error metric, the CF of a TIF is calibrated based on a reference surface error map containing a single sinusoidal frequency and a reference TIF derived from Preston's equation. Based on the novel Integrated PSD of a TIF metric, the method to generalize the calibrated CF to determine the sizes of different kinds of TIFs in typical CCOS processes is then presented, verifying the applicability of the method. Finally, the proposed idea is statistically studied with a well-designed computer simulation on many initial surface error maps and different combinations of CFRs. The simulation results demonstrate that the CFR = 0.75 consistently achieves the most stable balance among the residual error, total run time, and total number of iterations, and thus can be chosen as a simple criterion to guide the tool size selection.

DISCLOSURES

This thesis is a slightly modified version of a paper that will be published in a journal.

REFERENCES

Beaucamp, A. and Y. Namba (2013). Super-smooth finishing of diamond turned hard X-ray molding dies by combined fluid jet and bonnet polishing. *CIRP annals*, **62**(1), pp. 315–318.

Chaves-Jacob, J., A. Beaucamp, W. Zhu, D. Kono, and J.-M. Linares (2021). Towards an understanding of surface finishing with compliant tools using a fast and accurate simulation method. *International Journal of Machine Tools and Manufacture*, **163**, p. 103704.

Cheng, H. (2016). *Independent variables for optical surfacing systems*. Springer.

Dong, Z., H. Cheng, and H.-Y. Tam (2014). Modified subaperture tool influence functions of a flat-pitch polisher with reverse-calculated material removal rate. *Applied Optics*, **53**(11), pp. 2455–2464.

Fanson, J., R. Bernstein, G. Angeli, D. Ashby, B. Bigelow, G. Brossus, A. Bouchez, W. Burgett, A. Contos, R. Demers, F. Figueroa, B. Fischer, F. Groark, R. Laskin, R. Millan-Gabet, M. Pi, and N. Wheeler (2020). Overview and status of the Giant Magellan Telescope project. In *Ground-based and Airborne Telescopes VIII*, volume 11445, p. 114451F. International Society for Optics and Photonics.

Ghigo, M., G. Vecchi, S. Basso, O. Citterio, M. Civitani, E. Mattaini, G. Pareschi, and G. Sironi (2014). Ion figuring of large prototype mirror segments for the E-ELT. In Navarro, R., C. R. Cunningham, and A. A. Barto (eds.) *Advances in Optical and Mechanical Technologies for Telescopes and Instrumentation*, volume 9151, pp. 225 – 236. International Society for Optics and Photonics, SPIE.

Han, Y., F. Duan, W. Zhu, L. Zhang, and A. Beaucamp (2020). Analytical and stochastic modeling of surface topography in time-dependent sub-aperture processing. *International Journal of Mechanical Sciences*, **175**, p. 105575.

Jacobs, T. D., T. Junge, and L. Pastewka (2017). Quantitative characterization of surface topography using spectral analysis. *Surface Topography: Metrology and Properties*, **5**(1), p. 013001.

Jones, R. A. (1977). Optimization of computer controlled polishing. *Applied optics*, **16**(1), pp. 218–224.

Kim, D., H. Choi, T. Brendel, H. Quach, M. Esparza, H. Kang, Y.-T. Feng, J. N. Ashcraft, X. Ke, T. Wang, and E. S. Douglas (2021). Advances in Optical Engineering for Future Telescopes. *Opto-Electronic Advances*, pp. 210040–1.

Kim, D. W., S.-W. Kim, and J. H. Burge (2009a). Non-sequential optimization technique for a computer controlled optical surfacing process using multiple tool influence functions. *Optics express*, **17**(24), pp. 21850–21866.

Kim, D. W., C.-j. Oh, A. Lowman, G. A. Smith, M. Aftab, and J. H. Burge (2016). Manufacturing of super-polished large aspheric/freeform optics. In *Advances in Optical and Mechanical Technologies for Telescopes and Instrumentation II*, volume 9912, p. 99120F. International Society for Optics and Photonics.

Kim, D. W., W. H. Park, S.-W. Kim, and J. H. Burge (2009b). Parametric modeling of edge effects for polishing tool influence functions. *Optics Express*, **17**(7), pp. 5656–5665.

Schindler, A., T. Haensel, A. Nickel, H.-J. Thomas, H. Lammert, and F. Siewert (2003). Finishing procedure for high-performance synchrotron optics. In *Optical Manufacturing and Testing V*, volume 5180, pp. 64–72. International Society for Optics and Photonics.

Thiess, H., H. Lasser, and F. Siewert (2010). Fabrication of X-ray mirrors for synchrotron applications. *Nuclear Instruments and Methods in Physics Research Section A: Accelerators, Spectrometers, Detectors and Associated Equipment*, **616**(2-3), pp. 157–161.

Wang, J., B. Fan, Y. Wan, C. Shi, and B. Zhuo (2014). Method to calculate the error correction ability of tool influence function in certain polishing conditions. *Optical Engineering*, **53**(7), p. 075106.

Wang, J., X. Hou, Y. Wan, and C. Shi (2017). An optimized method to calculate error correction capability of tool influence function in frequency domain. In *Optifab 2017*, volume 10448, p. 104481Z. International Society for Optics and Photonics.

Wang, T., L. Huang, H. Choi, M. Vescovi, D. Kuhne, Y. Zhu, W. C. Pullen, X. Ke, D. W. Kim, Q. Kemao, K. Tayabaly, N. Bouet, and M. Idir (2021a). RISE: robust iterative surface extension for sub-nanometer X-ray mirror fabrication. *Optics Express*, **29**(10), pp. 15114–15132.

Wang, T., L. Huang, H. Kang, H. Choi, D. W. Kim, K. Tayabaly, and M. Idir (2020). RIFTA: A Robust Iterative Fourier Transform-based dwell time Algorithm for ultra-precision ion beam figuring of synchrotron mirrors. *Scientific Reports*, **10**(1), pp. 1–12.

Wang, T., L. Huang, M. Vescovi, D. Kuhne, Y. Zhu, V. S. Negi, Z. Zhang, C. Wang, X. Ke, H. Choi, W. C. Pullen, D. Kim, Q. Kemao, K. Nakhoda, N. Bouet, and M. Idir (2021b). Universal dwell time optimization for deterministic optics fabrication. *Optics Express*, **29**(23), pp. 38737–38757.

Weiser, M. (2009). Ion beam figuring for lithography optics. *Nuclear Instruments and Methods in Physics Research Section B: Beam Interactions with Materials and Atoms*, **267**(8-9), pp. 1390–1393.

Wischmeier, L., P. Graeupner, P. Kuerz, W. Kaiser, J. van Schoot, J. Mallmann, J. de Pee, and J. Stoeldraijer (2020). High-NA EUV lithography optics becomes reality. In *Extreme Ultraviolet (EUV) Lithography XI*, volume 11323, p. 1132308. International Society for Optics and Photonics.

Zhou, L., Y. Dai, X. Xie, and S. Li (2009). Frequency-domain analysis of computer-controlled optical surfacing processes. *Science in China Series E: Technological Sciences*, **52**(7), pp. 2061–2068.